

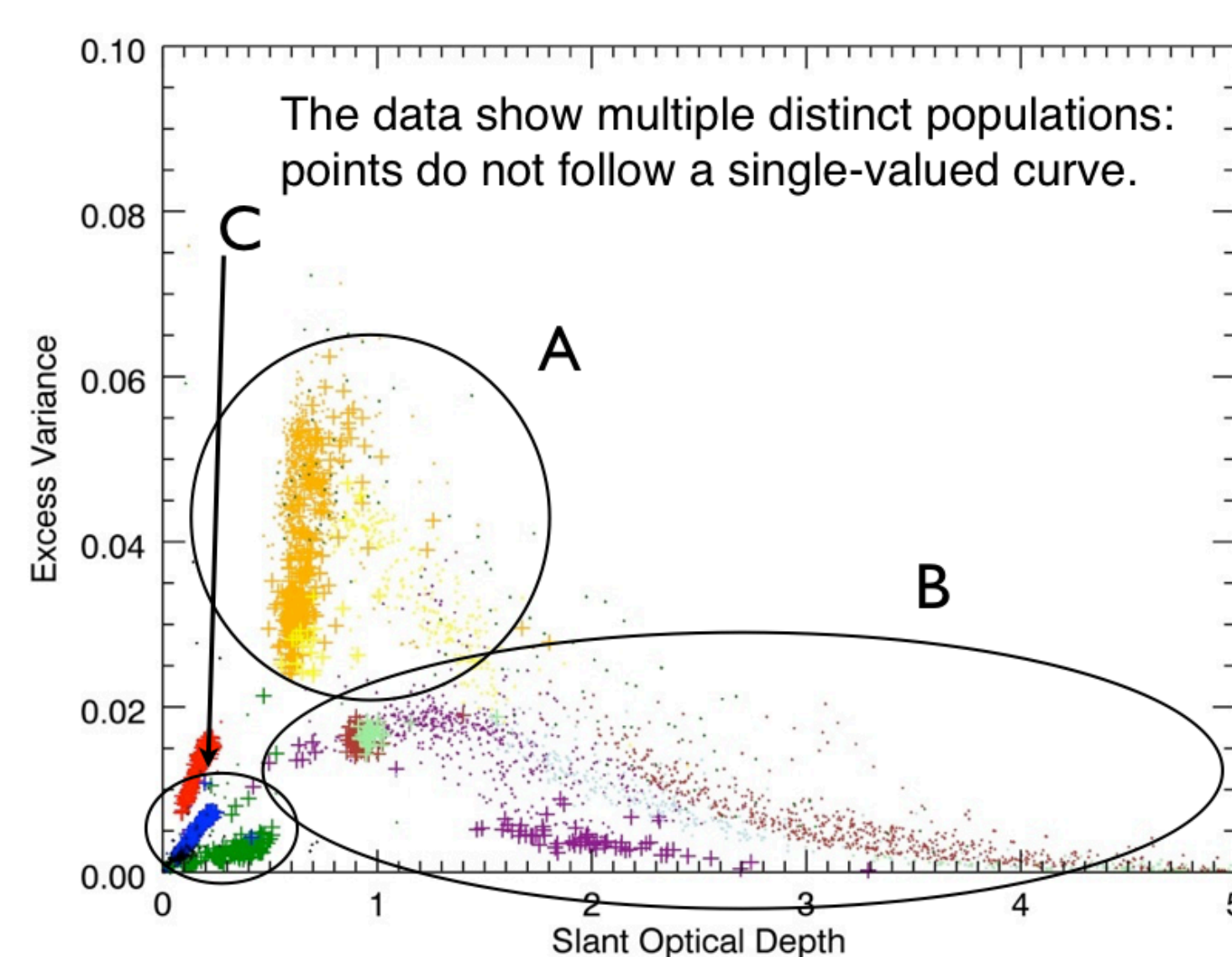
Particle Properties in Saturn's Rings from Skewness of Cassini UVIS Stellar Occultations

M. R. Green, J. Payne-Avary, J. H. Cooney, J. E. Colwell

University of Central Florida

Introduction

The Cassini UVIS High Speed Photometer measured stellar signals through Saturn's rings over a variety of viewing geometries, providing different line-of-sight optical depths for each location in the rings. In the absence of intervening ring material the data are described by Poisson counting statistics, and the excess variance can be used to provide a measure of particle or clump length scale in the rings (e.g. Colwell et al. 2018, Showalter and Nicholson 1990). The next higher moment of the occultation data, the skewness, has additional information about the distribution of particles and clumps on scales that are below the spatial resolution of the occultations. We carried out Monte Carlo simulations of various distributions of ring particles and simulated occultations through these simulated ring patches. We calculate the excess variance, skewness, and kurtosis for simulated occultations with different distributions of particle sizes and gaps. We find a relationship between skewness, S , and optical depth that varies with particle size, and have also simulated the effects of isolated features in the rings such as large clumps or gaps.



Fig(1)
 $E(\tau)$ for Beta Centaurii 771. Regions A, B and C correspond with rings A, B and C respectively. From this figure we can see that there are different populations of ring particles in different ring regions.

We carry out two sets of simulations, with and without gaps or “ghosts” (Baillié et al. 2013) in the rings. Particles are assumed to be spherical and uncorrelated with each other from integration period to integration period. We performed simulations with single-sized particles and with simple power-law size distributions:

$$n(r)dr = Cr^{-q}dr$$

where q is the power-law index, and $n(r)dr$ spans a range of particle sizes from $R1$ to $R2$. Particle radii are specified in terms of the size of the integration area, A , assumed to be a square of width 1 in the Monte Carlo simulations.

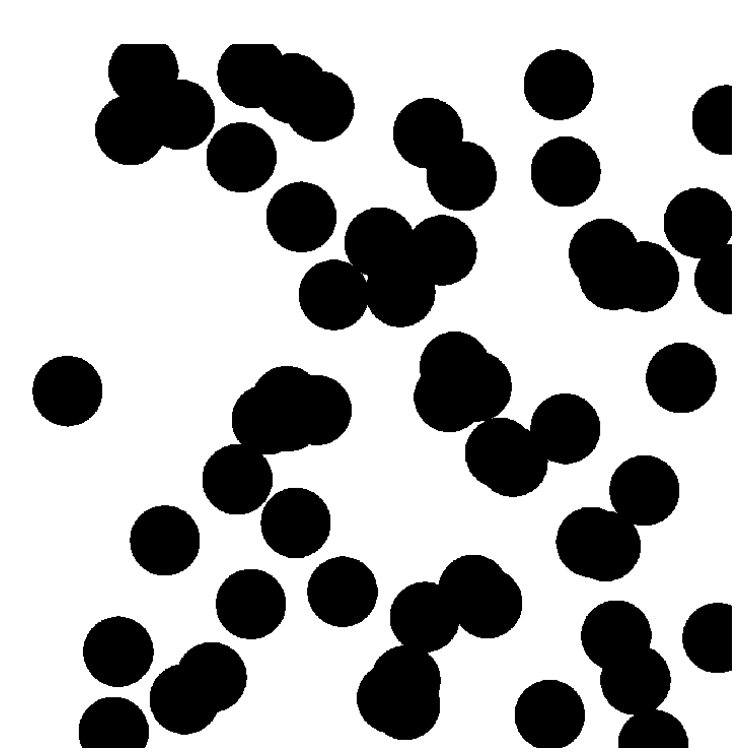
Simulations are run with 400 simulated data points. The star brightness is simulated as 500 photons per integration period. A typical resolution of for UVIS occultations is 10-20 m in ring plane radius per measurement, and the brightest stars observed had about 700 counts per integration period (Colwell et al. 2009). When ghosts are introduced, a particle-free integration area is introduced with a probability of gp .

Results

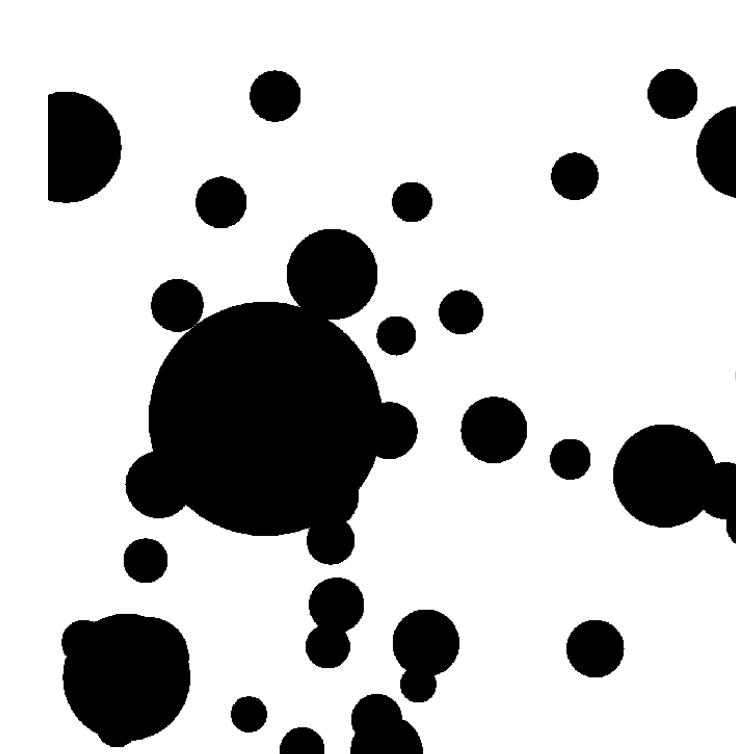
Below are simulations of a single integration frame, two with a single particle size, $R=0.01$ and $R=0.05$, and the other with power-law distributed particle size, where $R1=0.025$, $R2=0.2$, and $q=3.1$. The simulated star brightness is 500 counts, and the optical depth is ~ 0.37 .



Fig(2)
Integration frame where particles are all the same size, $R=0.01$. A simulation of 4000 points with these particles gave $E=7.43e-05$, $S=0.015$, $K=0.033$.

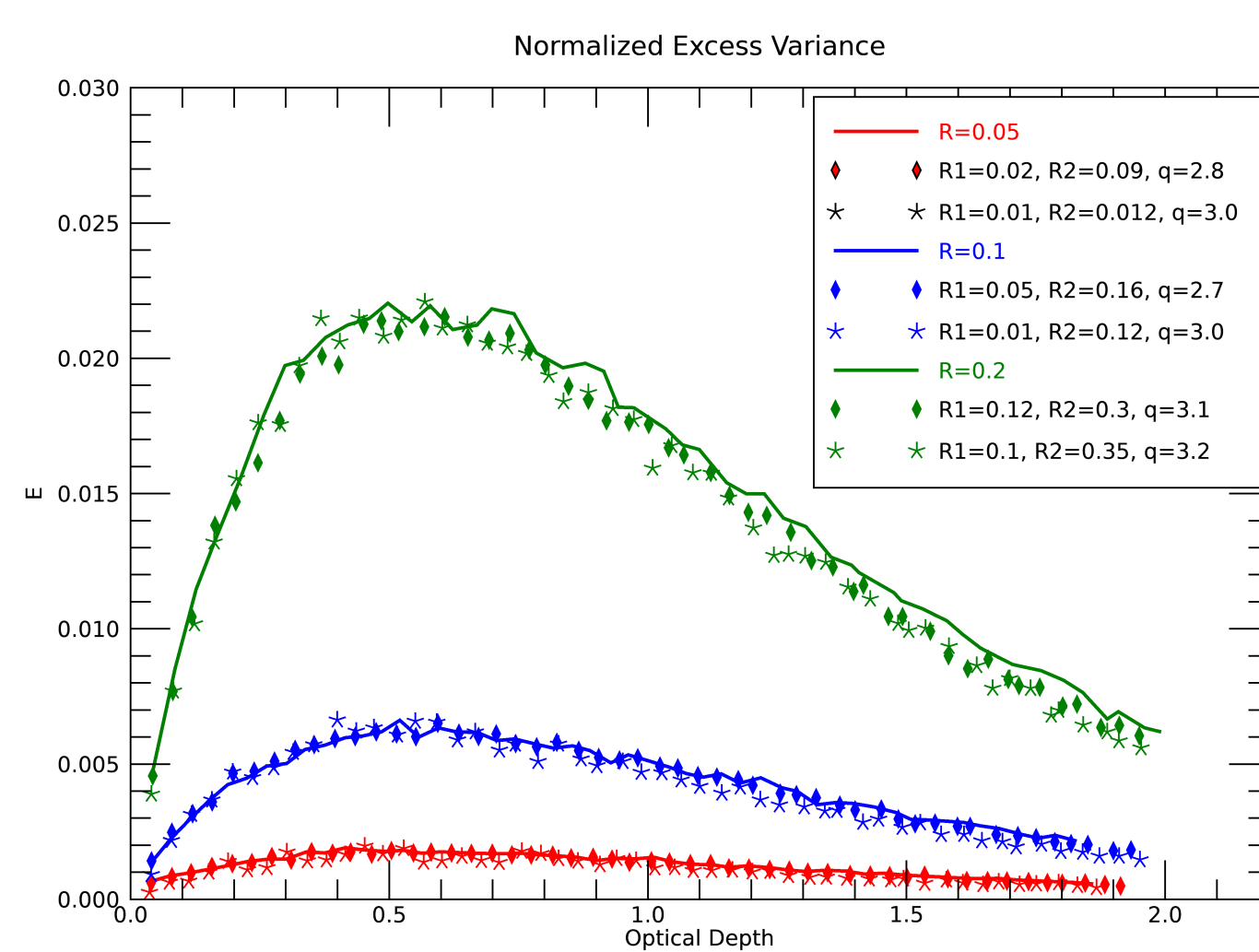


Fig(3)
Integration frame where particles are all the same size, $R=0.05$. A simulation of 4000 points with these particles gave $E=0.0015$, $S=0.059$, $K=0.19$.

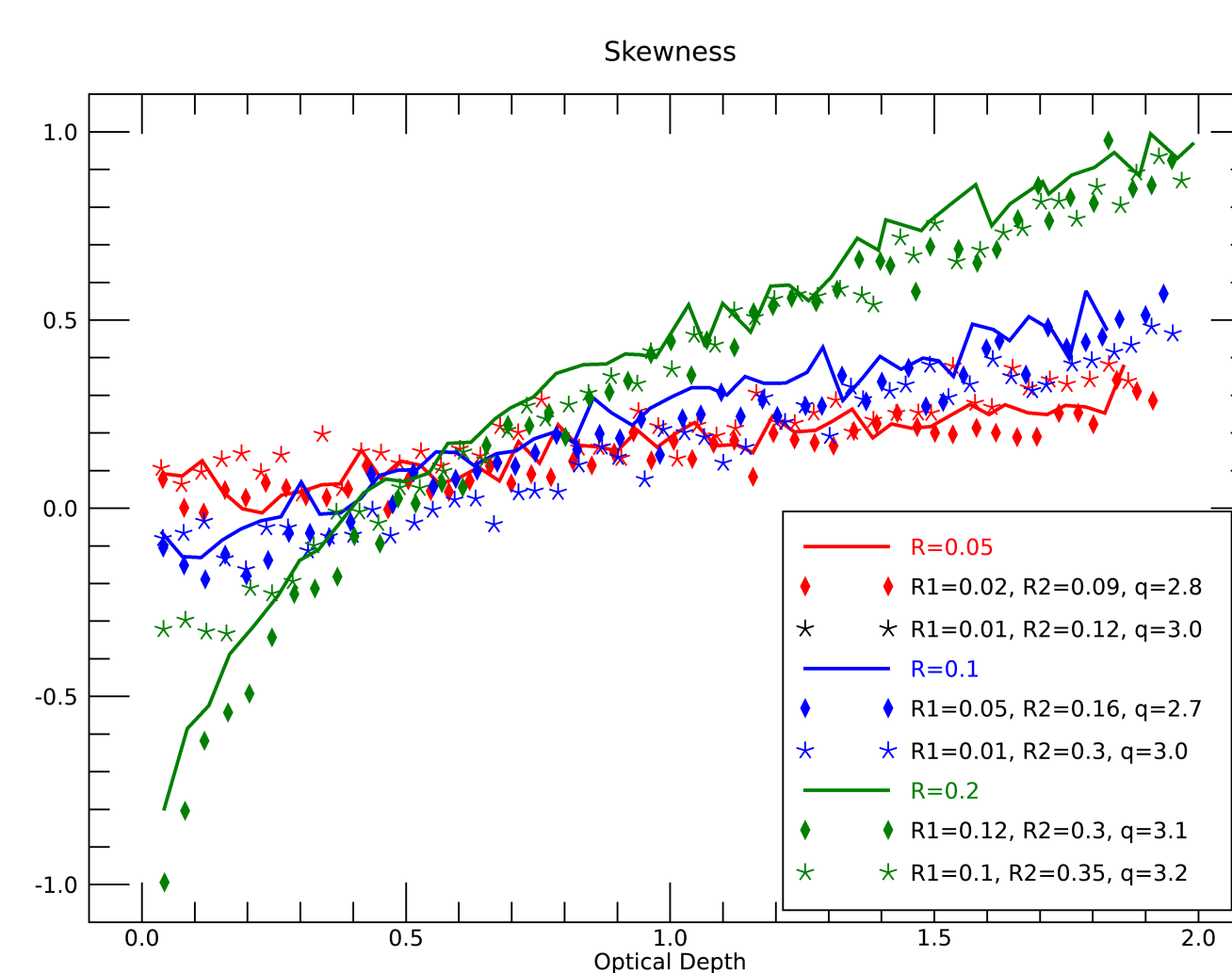


Fig(4)
Integration frame where particles obey a power-law size distribution, where $R1=0.025$, $R2=0.2$, and $q=3.1$. A simulation of 4000 points with these particles gave $E=0.0044$, $S=-0.16$, $K=0.012$.

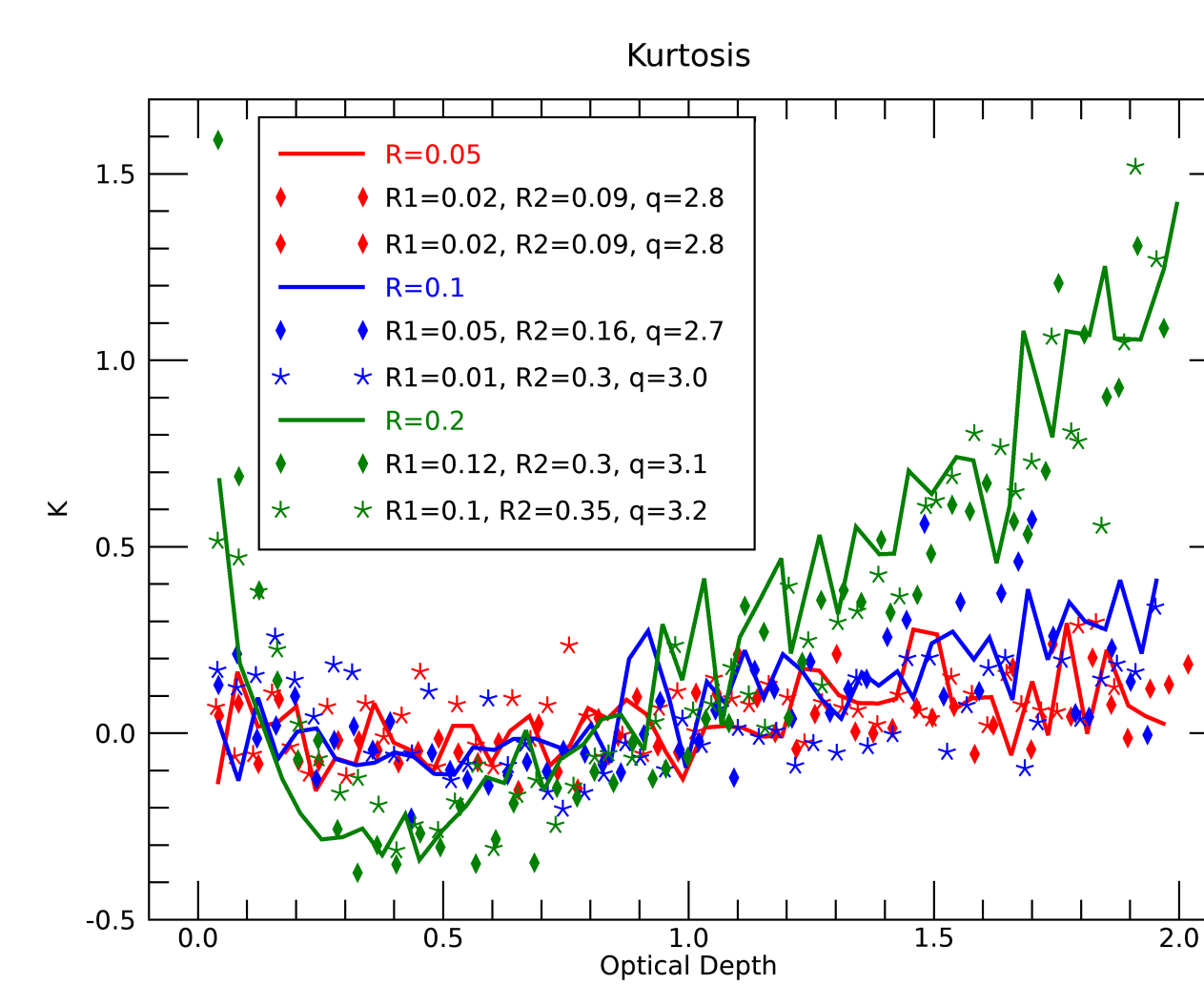
We carried out simulations with single-sized particles and with power-law size distributions. We were able to find a single value of particle size, R , that produces the same distributions of $E(\tau)$, $S(\tau)$, and $K(\tau)$ as a power-law size distribution. Thus, while the statistical moments can be shown to be consistent with a power-law size distribution, they are diagnostic of a single effective particle or clump size.



Fig(5)
 $E(\tau)$ for various particle size distributions.

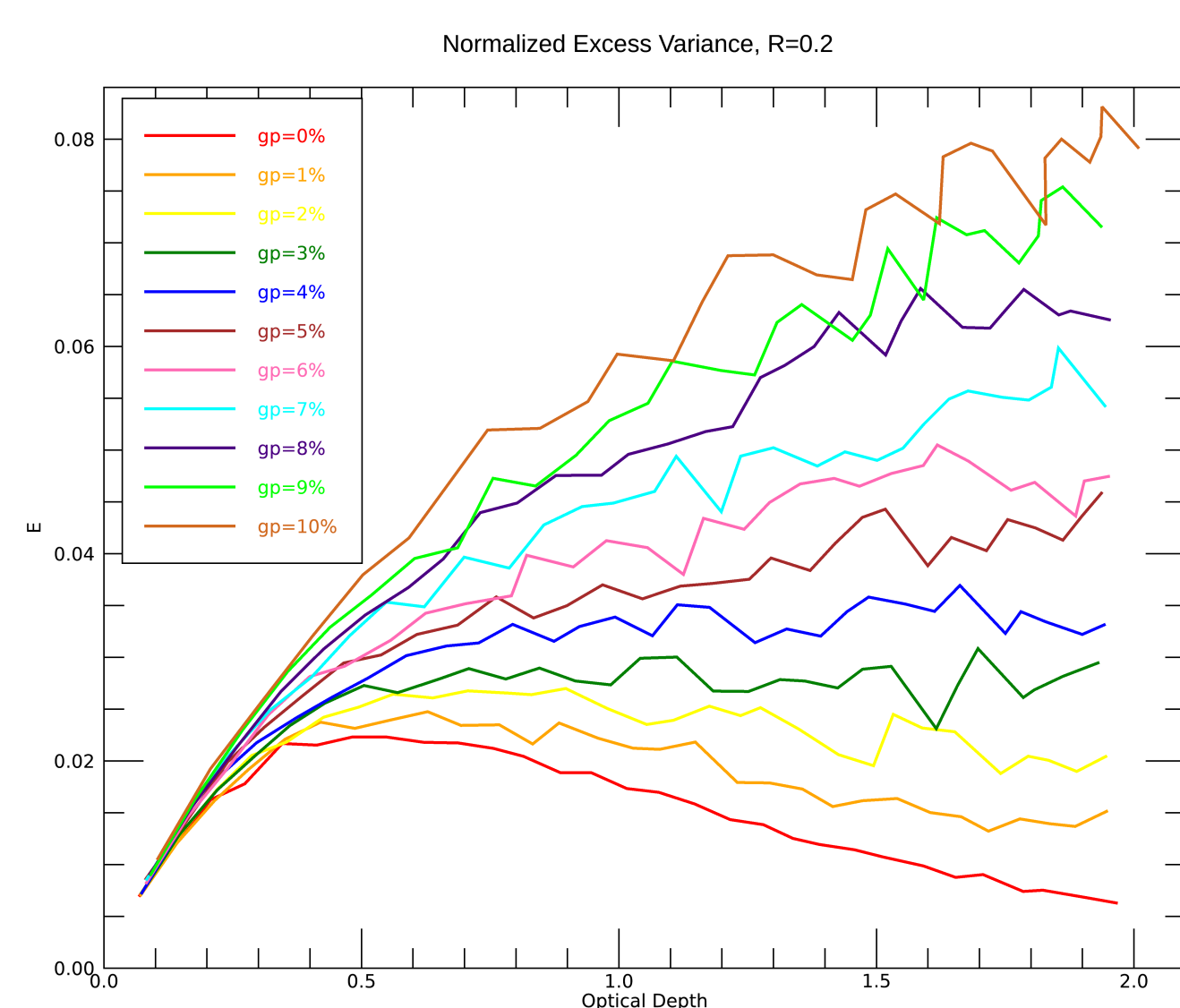


Fig(6)
 $S(\tau)$ for various particle size distributions.

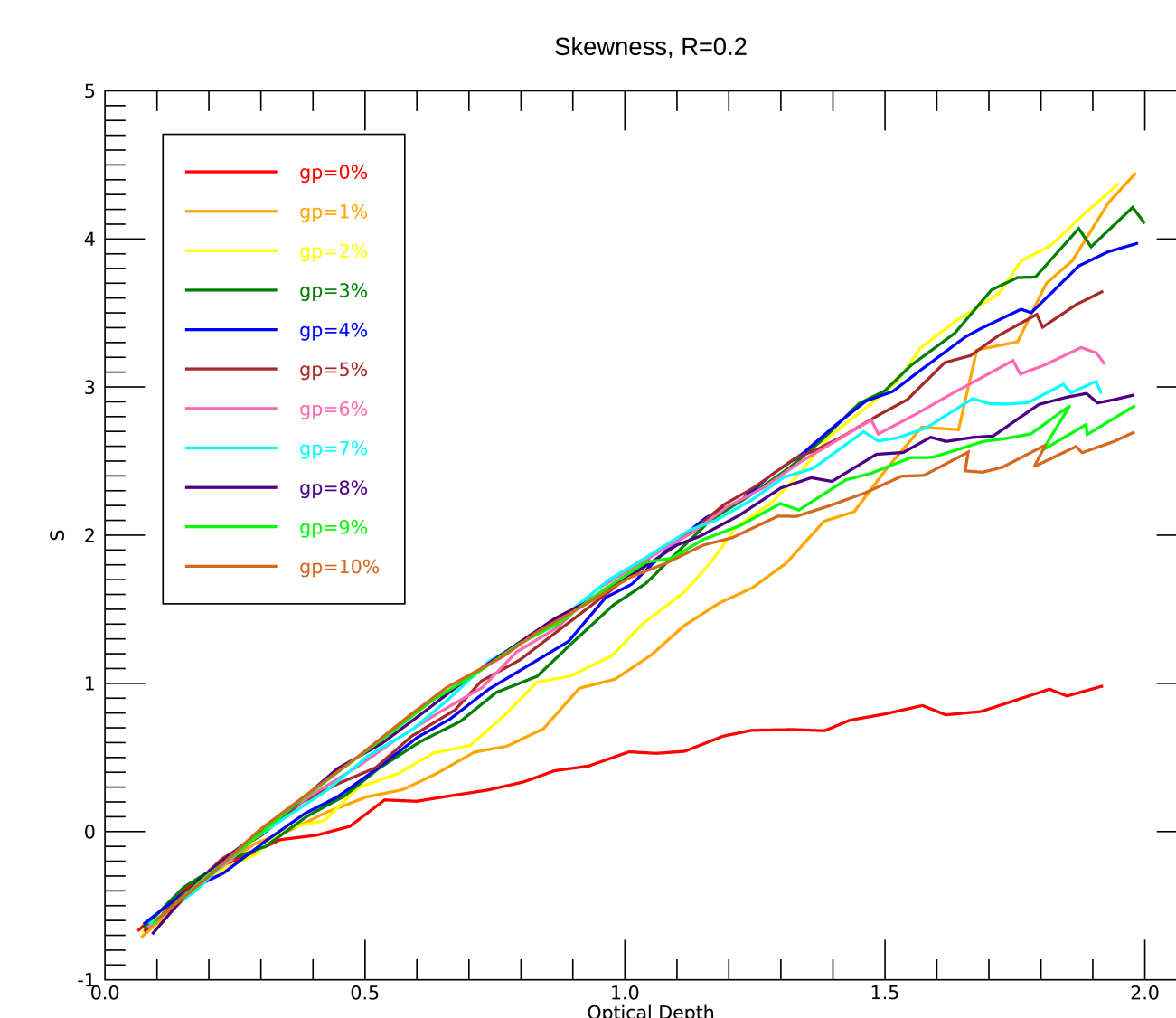


Fig(7)
 $K(\tau)$ for various particle size distributions.

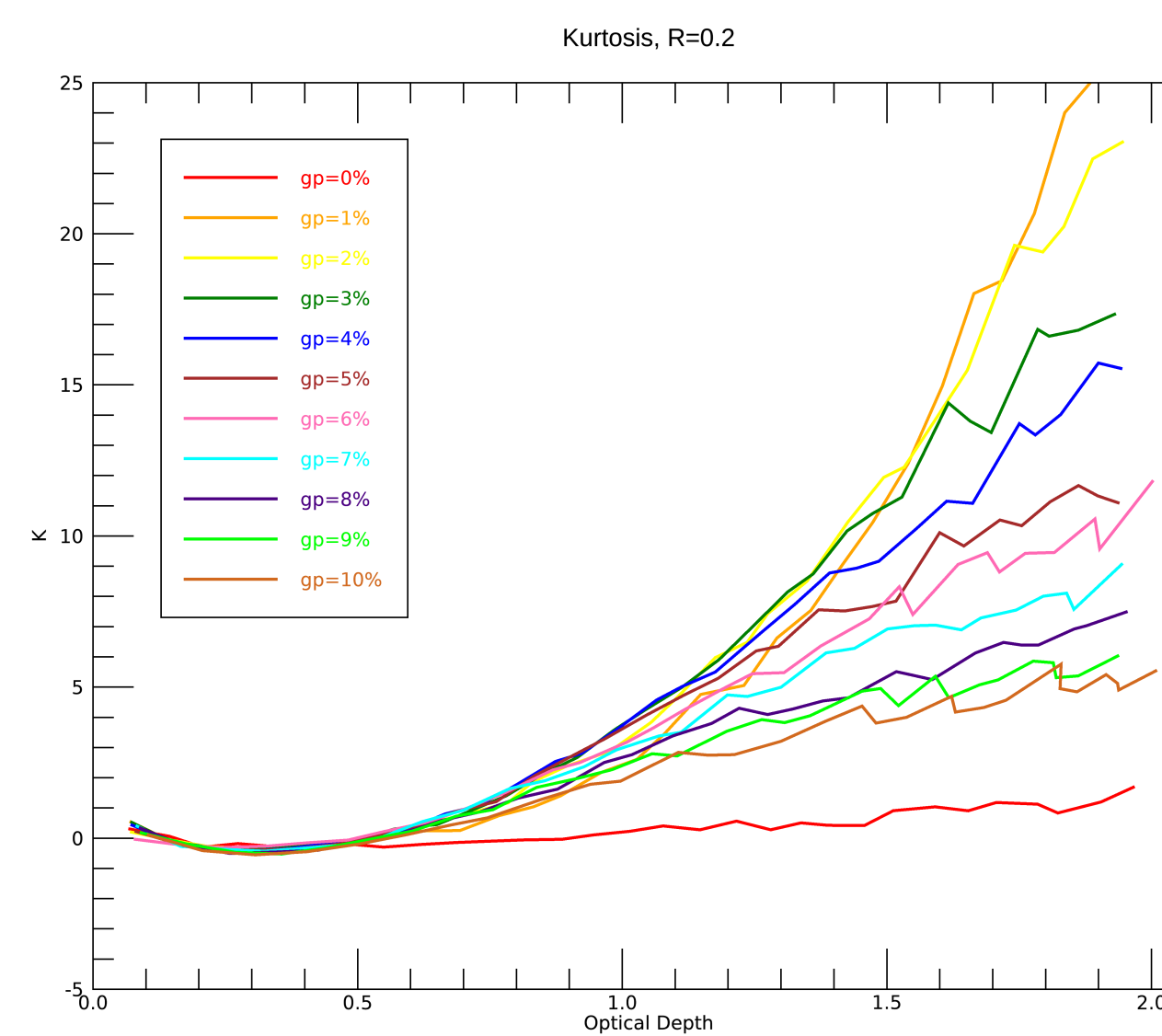
The parameter gp (for ghost probability) is the fraction of integration frames that are empty in a simulation to simulate the “ghosts” or localized gaps seen in occultation data (Baillié et al. 2013). These plots show how all three moments change as gp increases. The most prominent feature here is that $E(\tau)$ starts losing its expected shape as the ghost parameter increases.



Fig(8)
Normalized Excess Variance as a function of optical depth for a single particle size of $R=0.2$. $E(\tau)$ seems to lose its expected shape after the ghost parameter is introduced.



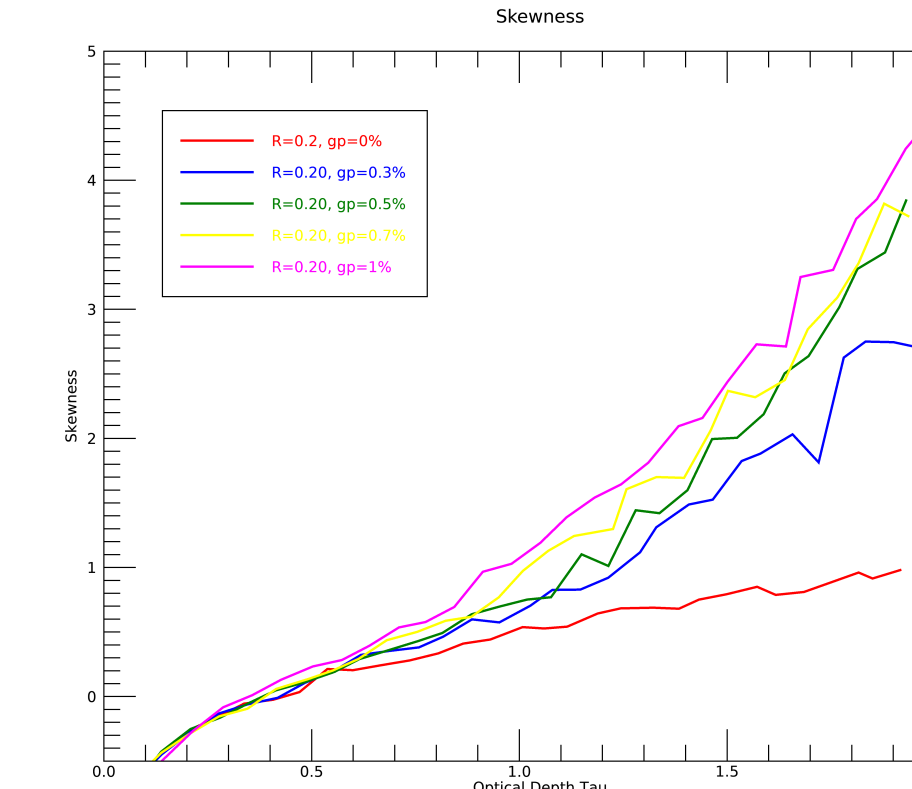
Fig(9)
Skewness as a function of optical depth for a single particle size of $R=0.2$. $S(\tau)$ increases with gp for lower optical depths. For higher optical depths $S(\tau)$ jumps from $gp=0\%$ to 1% , then decreases as gp approaches 10% .



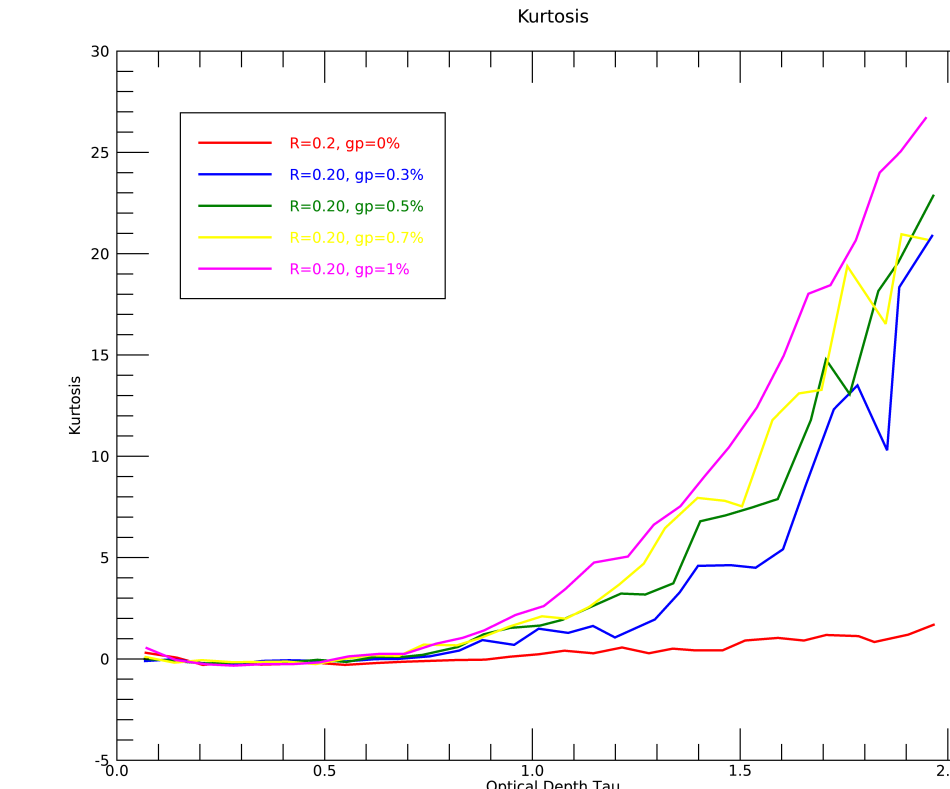
Fig(10)
Kurtosis as a function of optical depth for a single particle size of $R=0.2$. Much like skewness, $K(\tau)$ increases with gp for lower optical depths, and has the jump from $gp=0\%$ to 1% , while decreasing between 1% and 10% .

Results

For $S(\tau)$ and $K(\tau)$ we see a jump from $gp = 0\%$ to 1% , so the following plots show these moments for three values of gp between 0 and 1, to help us gain insight to why such jumps exist.



Fig(11)
Skewness as a function of optical depth for a single particle size of $R=0.2$, for values of gp between 0% and 1% . At these low gp levels, $S(\tau)$ increases with gp , over the entire range of optical depths.



Fig(12)
Kurtosis as a function of optical depth for a single particle size of $R=0.2$. Again, $K(\tau)$ increases with gp , over all values of τ .

Conclusions

Patterns in Excess Variance

- As gp increases, $E(\tau)$ increases, over all values of R
- We do not see the jump from $gp = 0\%$ to 10% that is seen in the $S(\tau)$ and $K(\tau)$ plots
- $E(\tau)$ loses its expected shape after $gp=1\%$
- Between $gp=0\%$ and 1% , $E(\tau)$ increases with increasing gp

Patterns in Skewness:

- For low optical depths (0.5 and lower), $S(\tau)$ increases with increasing gp
- For higher optical depths (above 0.5), $S(\tau)$ jumps from 0% gp to 1% gp , then decreases as gp increases
- Between 0% and 1% gp , $S(\tau)$ increases as gp increases

Patterns in Kurtosis:

- For low optical depths (0.5 and lower), $K(\tau)$ increases with increasing gp
- For higher optical depths (above 0.5), $S(\tau)$ jumps from 0% gp to 1% gp , then decreases as gp increases
- Between 0% and 1% gp , $K(\tau)$ increases as gp increases

There are multiple values for $R1$, $R2$, and q that can yield plots of all three higher order moments that are identical to the same plots produced using a single particle size. The statistical moments of the UVIS stellar occultations can be explained by a single particle or clump size. However, the presence of ghosts and other large-scale clumps or structure in the rings produce changes in the distributions of the statistical moments. Thus, analysis of these moments can provide information not only on an effective particle size but also the mesoscale structure of rings including self-gravity wakes, localized gaps or “ghosts”, viscous overstabilities, and other unresolved or marginally resolved structures and patterns in the rings.

Future steps include exploring a so-called ‘anti-ghost’ parameter, a counter part to gp that simulates clumping, and simulating regions with multiple ring populations as seen in fig (1). Exploring $E(\tau)$'s devolution for increasing gp would serve as a useful next step as well.

References

- Colwell, J. E., Esposito, L. W., Cooney, J. H., Icarus, 300, 150-166
Showalter, Mark R., Nicholson, Philip D., Icarus, 87, 285-306
Baillié, Kévin; Colwell, Joshua E.; Esposito, Larry W.; Lewis, Mark C., ApJ, 145, 171